Adv Polym Sci (2010) 223: 29–44
DOI:10.1007/12_2009_5

Published online: 19 June 2009

Effective Temperature Models for the Electric Field Dependence of Charge Carrier Mobility in Tris(8-hydroxyquinoline) Aluminum

P.J. Jadhav, B.N. Limketkai, and M.A. Baldo

Abstract The development of accurate and predictive models of charge carrier mobility is a crucial milestone on the path to the rational design of organic semiconductor devices. In this chapter we review effective temperature models that combine both the temperature and electric field dependence of the charge carrier mobility into a single parameter – the effective temperature. Although effective temperature models were originally developed for use in disordered inorganic semiconductors, here we compare various models to data from the archetype small molecular weight organic semiconductor tris(8-hydroxyquinoline) aluminum (AlQ_3). We conclude that it may prove impossible to develop a universal effective temperature model that is valid for all electric fields and temperatures. But several effective temperature models are observed to work well within the typical operational environments of electronic devices. Thus, the effective temperature concept promises to be a practical and useful tool for the development of organic semiconductor technology.

Contents

P.J. Jadhav, B.N. Limketkai, and M.A. Baldo (✉)
Department of Electrical Engineering and Computer Science, Massachusetts Institute of Technology, Cambridge, MA 02139, USA
e-mail:baldo@mit.edu

1 Introduction

Organic semiconductor-based devices such as organic light emitting devices (OLEDs) are attracting increasing commercial interest. Unlike most conventional semiconductors, however, the molecules in an organic semiconductor are held together by weak van der Waal's forces. Consequently, organic semiconductors possess narrower electronic bands than most conventional covalently-bonded semiconductors. The result is localization of charge carriers [1], especially in the disordered amorphous organic semiconductors typical of applications such as OLEDs.

Localized charge carriers in organic semiconductors move by electric field or temperature-induced charge hopping. There are proven microscopic models for charge hopping between sites under low electric fields [2–4]. But charge transport in thin films of organic semiconductors is complicated by energetic and spatial disorder. For example, the conductivity of a thin film is observed to depend on the charge carrier density as well as the electric field and temperature [5–10]. The absence of an analytical model that explains all these dependencies has complicated the rational design of organic semiconductor devices.

The modeling of charge carrier transport in organic semiconductors has been dominated by quasi-empirical models such as the various Poole Frenkel descriptions for the electric field dependence of mobility [9, 11]. But empirical relations complicate the construction of predictive device models because many parameters are of obscure physical origin and difficult to extrapolate between materials. This chapter reviews an alternative approach: effective temperature models. These modify the distribution of charge carriers, increasing their temperature to represent the effect of an applied electric field. We present comparisons to organic semiconductor data that demonstrate the utility of the effective temperature approach for device engineers. It correctly models device behavior near room temperature, and the physical origin and limits of the approach are clear.

Much of the theory discussed here was originally proposed many years ago for application to disordered conventional semiconductors such as amorphous Si [12–15]. We review effective temperature models that build on the success of percolation theory in understanding the charge density and temperature dependence of charge transport. Percolation theory at low electric field is reviewed in Sect. 2. To summarize: percolation theory in the absence of an electric field predicts that mobility is strongly dependent on the charge carrier density [10]. Given the presence of just a few charge carriers, the current flow is retarded by sparsely distributed low energy sites also known as traps. The mobility of carriers increases dramatically as these deep sites are filled. Because the majority of hops out of a trap are to sites with higher energy, the mobility is also strongly temperature dependent. Given an exponential density of states (DOS), the theory predicts $\mu \sim n^{T_0/T}$ where μ is the mobility, n the charge carrier density, T the temperature, and T_0 the characteristic trap temperature [10]. Interestingly, this solution is almost identical to the successful but controversial trapped charge limited (TCL) model for charge transport in organic semiconductors [5, 16, 17], although percolation theory correctly models

the localized nature of organic semiconductors whereas the TCL models consider an unphysical band edge above an exponential distribution of traps.

Percolation models in the absence of an electric field have previously proven successful in organic thin film transistors where the lateral electric field in the channel can comfortably be neglected due to the large dimensions of the channel [10]. The electric field, however, is typically much larger in thin vertical organic devices such as OLEDs or organic photovoltaics (OPVs). Large electric fields lead to a nonequilibrium distribution of charge carriers that can prove difficult to model. In response, the effective temperature model notes that the effect of electric field on mobility in hopping transport is similar to that of temperature [15, 18, 19]. Increasing the temperature raises the population of charge carriers to higher energies, where the DOS is broader, and hence the mobility improves. Increasing the field has a similar effect – the carriers gain energy by hopping in the direction of the field. So the mobility can be seen as dependent on some quantity $T_{\text{eff}}(F,T)$, which is a function of electric field and temperature. We define $T_{\text{eff}}(F,T)$ as the effective temperature. The form of the function $T_{\text{eff}}(F,T)$ is the subject of Sect. 3 of this chapter.

In Sect. 4 we compare the various effective temperature theories to current–voltage and mobility data for organic semiconductors. We focus particularly on analysis of the current–voltage characteristics of the archetype small molecular weight electron transport material tris(8-hydroxyquinoline) aluminum (AlQ_3) [20]. There is extensive data available on the charge transport characteristics of AlQ_3 [5, 21–23], providing a convenient system to test various approaches to modeling charge transport in disordered organic semiconductors. Finally, in Sect. 5, we conclude by discussing the limits of the effective temperature approach.

2 Percolation Models of Mobility at Low Electric Fields

Percolation models of charge conduction were originally applied to charge transport in inorganic amorphous semiconductors [12]. More recently the percolation formalism has also been applied to organic materials [10, 24]. Here, we review the percolation approach. It begins by noting that charge transport in organic semiconductors occurs via electric field or thermally-activated hops between localized states. The hopping motion of charge carriers can be described by the kinetic master equation [25]

$$\frac{\partial P_{\text{d}}(t)}{\partial t} = \sum_{\text{a}\neq\text{d}} \left[R_{\text{da}} P_{\text{d}}(t)\left(1-P_{\text{a}}(t)\right) - R_{\text{ad}} P_{\text{a}}(t)\left(1-P_{\text{d}}(t)\right)\right], \tag{1}$$

where $P_{\text{d}}(t)$ is the occupational probability of site d at time t and R_{da} is the transition rate from the donor site d to acceptor site a.

Next, we assume that polaronic effects are negligible compared to energetic disorder. The activation energy ΔE for hopping is then dependent only on the site energy differences and not on the molecular conformation energies required to form activated complexes prior to charge transfer. Under this assumption, the hopping rate

R_{da} from a site with energy E_d to a site with energy E_a at a distance r_{da} apart can be described by the Miller–Abrahams rate model for phonon-assisted tunneling [2]:

$$R_{da} = \begin{cases} \nu_0 \exp(-2ar_{da}) \exp((E_a - E_d)/kT), & E_a - E_d > 0, \\ \nu_0 \exp(-2ar_{da}), & E_a - E_d \leq 0, \end{cases} \tag{2}$$

where ν_0 is the attempt to hop frequency dependent on the phonon DOS and intermolecular overlap. Miller Abrahams is perhaps the simplest solution that satisfies the detailed balance requirement in Eq. (1) at equilibrium.

Under the condition that the system is close to equilibrium (i.e., the difference between donor and acceptor quasi Fermi levels $\mu_d - \mu_a \ll 2kT$), the master equation with Miller–Abrahams transition rates can be linearized to obtain a conductance [26]:

$$G_{da} = \frac{q\nu_0}{4kT} \frac{\exp[-2\alpha r_{da}] \exp\left[-|E_a - E_d|/2kT\right]}{\cosh\left[(E_a - \mu_a)/2kT\right] \cosh\left[(E_d - \mu_d)/2kT\right]}. \tag{3}$$

Here, μ_d and μ_a are the quasi-electrochemical potentials that deviate from the equilibrium electrochemical potential as $\mu - qFr$, where μ is the chemical potential, F is the applied field, and r is the position of the sites.

Equation (3), or a simplified version thereof, can be used to model every possible hop between localized sites in the organic semiconductor as a distinct conductance. Each conductance is characterized by the respective site energies, the intermolecular spacing and the quasi Fermi energies. Unfortunately, the energy distribution of the sites (also known as the DOS) is usually unknown because, until recently, it has not been easy to measure. It is commonly presumed to be a Gaussian distribution [11] with a tail of states that extends into the energy gap between the lowest unoccupied molecular orbital (LUMO) and the highest occupied molecular orbital (HOMO). Recent Kelvin probe measurements of the archetype organic semiconductors N,N'-diphenyl-N,N'-bis(1-naphthyl)-1,1′-biphenyl–4,4′-diamine (α-NPD) [27], and copper phthalocyanine (CuPC) [28], however, have observed an exponential DOS. In this chapter, we tentatively assume that exponential tails are a universal characteristic of organic semiconductors. Further measurements of other archetype organic semiconductors may confirm this assumption. Disorder in the intermolecular spacing is usually neglected since it is expected to yield a charge carrier mobility that decreases with electric field, in contrast with experimental results [11, 29].

Assuming we know the distribution of site energies, and if we neglect the spatial disorder, the remaining problem is to solve the conductance network. In an organic semiconductor the conductances corresponding to each possible hop are expected to vary by many orders of magnitude. Percolation theory seeks to simplify the determination of the macroscopic conductance in this disordered system [12, 30]. Conceptually, the film is broken into numerous conducting clusters defined relative to a reference conductance G. For a given reference conductance G, all conductive pathways between sites with $G_{da} \leq G$ are removed from the network, which leaves a collection of spatially disconnected clusters of high conductivity, $G_{da} > G$. As the reference conductance G is decreased, the size of these isolated clusters increases. The critical percolation conductance is defined as the maximum reference

conductance $G = G_c$ at the point when percolation first occurs, meaning the first formation of a continuous, infinite cluster (cluster that spans the whole system). This infinite cluster will be composed of clusters that are all connected by critical conductive links with conductance G_c. Since the conductances comprising the infinite cluster are expected to vary by many orders of magnitude, it is assumed that the conductivity of the cluster is that of the most resistive link. The total conductance of the system is then equal to G_c. To determine the threshold for percolation, the average number of bonds per site is calculated. A bond is defined as a link between two sites which have a conductance $G_{da} > G$. As the reference conductance G decreases, the average number of bonds per site B increases. A large average number of bonds per site indicates a large average size of a cluster (collection of sites with $G_{da} > G$). Therefore, it is assumed that once the average number of bonds per site B reaches some critical bond number B_c, the average cluster sizes will be large enough such that they all touch and form a continuous pathway that spans the whole disordered system (form an infinite cluster). The critical bond number is usually determined using numerical simulations. It has been estimated to be $B_c \simeq 2.8$ in an amorphous three-dimensional system [31].

To apply percolation theory, Eq. (3) is simplified by noting that bonds at the critical conductance involve site energies that are high above the quasi-electrochemical potential $(E_d - \mu_d \gg kT)$. The conductance in Eq. (3) for small applied electric fields can then be approximated in the zero-field limit as [26]

$$G_{da} \approx \frac{q\nu_0}{kT} \exp\left[-2\alpha r_{da}\right] \exp\left[-\frac{|E_a - E_d| + |E_d - \mu_d| + |E_a - \mu_a|}{2kT}\right]. \tag{4}$$

Next, the conductance between sites can be written as $G = G_0 \exp\left[-s_{ij}\right]$ with $G_0 = q\nu_0 / kT$ and [10]

$$s_{da} = 2\alpha r_{da} + \frac{|E_a - E_d| + |E_d - \mu_d| + |E_a - \mu_a|}{2kT}. \tag{5}$$

The critical conductance is written $G_c = G_0 \exp\left[-s_c\right]$. The conductivity of the disordered system is therefore $\sigma = \sigma_0 \exp\left[-s_c\right]$, where s_c is the critical exponent of the critical conductance when percolation first occurs (when $B = B_c$).

The average number of bonds B is equal to the density of bonds, N_b, divided by the density of sites that form bonds, N_s, in the material. At the percolation threshold, when $B = B_c$, the density of bonds is given by

$$N_b = \int d^3 r_{da} \int dE_d \int dE_a g\left(E_d\right) g\left(E_a\right) \theta\left(s_c - s_{da}\right), \tag{6}$$

where r_{ij} is integrated in three dimensions over the entire material, $g\left(E\right)$ is the DOS in the material, and θ is the Heaviside unit step function. The density of sites that form bonds at the percolation threshold $(B = B_c)$ is given by

$$N_s = \int dE g\left(E\right) \theta\left(s_c - s_{da}\right). \tag{7}$$

Determination of the conductance at the percolation threshold rests on the evaluation of step function. Setting $s_{da} = s_c$ in Eq. (5) yields either (1) a maximum hop distance, $r_{max} = s_c/2\alpha$, obtained when $E_a = E_d = \mu_a = \mu_d$, or (2) a maximum energy, $E_{max} = \mu + s_c kT$ in the limit of $r_{da} \to 0$. The maximum energy is crucial. Because the hops typically take place in the tail of the DOS, the maximum number of density of sites in the percolation cluster occurs at E_{max}. Consequently, it characterizes the system and sets the integration limits in Eqs. (6) and (7).

Assuming an exponential DOS with characteristic temperature T_0, Vissenberg and Matters [10] obtained

$$B_c = \frac{N_b}{N_s} \approx \pi N_0 \left(\frac{T_0}{2\alpha T}\right)^3 \exp\left[\frac{E_F + s_c kT}{kT_0}\right], \tag{8}$$

where they assumed $E_F \ll kT_0$ and $s_c kT \gg kT_0$ Solving for the critical conductance yields

$$\sigma = \sigma_0 e^{-s_c} = \sigma_0 \left[\frac{\pi}{B_c}\left(\frac{T_0}{2\alpha T}\right)^3 n\right]^{T_0/T}, \tag{9}$$

where n is the charge carrier density. Again, we stress that this result is largely a recapitulation of previous studies. Indeed, Vissenberg and Matters remarked that their result in Eq. (8) is in agreement with previous results up to a numerical factor [10]. Perhaps surprisingly, given their contrasting physical foundations, Eq. (9) is also identical to the TCL model up to a numerical factor [5, 16].

3 Effective Temperature Models

The result of the previous section is only valid close to equilibrium. The electric field is limited such that the difference between donor and acceptor quasi Fermi levels $\mu_d - \mu_a \ll 2kT$. Close to equilibrium we can assume that the electron distribution is characterized by the lattice temperature, and we can also linearize the hopping conductivity expression of Eq. (3).

Although the low electric field percolation model is useful in organic field effect transistors, it is not suitable for OLEDs or OPVs due to the much larger electric fields in these devices. Under an applied electric field, charge carriers hop from sites deep in the DOS to higher energy levels where the DOS is broader (see Fig. 1). The effect of the electric field is to create a population of "hot" carriers above the Fermi level [18]. The aim of the effective temperature concept is to model the electric field by a nonequilibrium distribution of electrons characterized by an effective temperature T_{eff}.

We expect T_{eff} to be a function of the temperature T and electric field F. The simplest cases are $F = 0$ and $T = 0$. The former is trivial: $T_{eff} = T$, and the expression

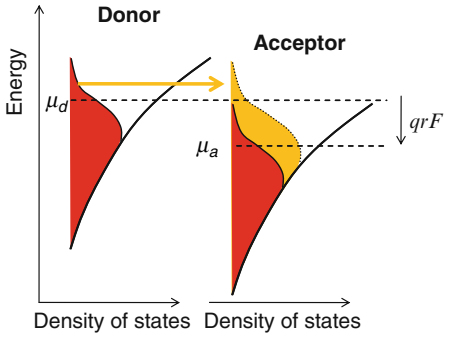

Fig. 1 Electron hopping within the energetic tail of a distribution of localized sites under an electric field F. Due to the potential gradient, electrons from lower energy states can hop into states further from the Fermi energy where the density of states is broader, and hence gaining energy with respect to the local Fermi level

for mobility should reduce to the proven low field percolation model. At $T = 0$, however, $T_{\text{eff}} = T_{\text{F}}$ where $T_{\text{F}} = qF/2\alpha k, q$ is the electronic charge, F is the *magnitude* of the electric field, α is the inverse of the decay length of the localized wave functions and k is the Boltzmann constant. Marianer et al. [18] have a simple approach to this result. When an electric field is applied at $T = 0$K, an electron can increase its local energy E by $\Delta E = qFr$ by hopping against the field over a distance r. The hopping mechanism at $T = 0$ is tunneling, and so the hopping rate into the acceptor state is

$$\nu = \nu_0 \exp(-2\alpha r) = \nu_0 \exp\left(-2\alpha \Delta E \,/ qF\right), \quad \Delta E > 0. \tag{10}$$

Marianer et al. [18] assume that "The energy relaxation rate does not depend exponentially on the energy difference." Consequently, we assume that relaxation from the hot state is independent of energy:

$$\nu = \nu_0, \quad \Delta E < 0. \tag{11}$$

To obtain the carrier distribution, we can label the relaxed state as the donor and the hot state as the acceptor. For steady state current flow between donor and acceptor states, the population of the donor and acceptor states should be invariant in time. Substituting Eqs. (10) and (11) into Eq. (1) is consistent with a Fermi–Dirac distribution with $T = T_{\text{F}} = qF \,/ 2\alpha k$.

Alternatively, we may obtain $kT_{\text{F}} = qF/2\alpha$ by demanding self consistency within a percolation cluster at $T = 0$. At $T = 0$, the percolation limit is given by Eq. (1) assuming no backward hops [24]:

$$f(E_{\text{c}}) \exp[-2\alpha r_{\text{da}}] = \exp[-s_{\text{c}}], \tag{12}$$

where E_{c} is the maximum donor energy and we have neglected filled acceptor sites in the tail of the distribution.

We are concerned with the carrier distribution $f(E_{\text{c}})$ at energies approaching the maximum possible donor energy E_{max}. From Eq. (12), $f(E_{\text{max}}) = \exp[-s_{\text{c}}]$. Because there is no thermal excitation at $T = 0$, carriers at E_{max} must be excited

by the electric field. Thus, sites at E_{max} must participate in bonds of length $r_{da} > 0$. It follows that, for short hops, the maximum acceptor energy cannot be less than E_{max}. The maximum acceptor energy is obtained by hops parallel to the electric field. Thus, for carriers with energy close to E_{max}, the percolation limit is

$$E_c = E_{max} - qr_{da}F. \tag{13}$$

For $T = 0$, Eqs. (12) and (13) yield an occupation function $f(E_c)$ of the form $A\exp[-E_c/kT_F]$, where $kT_F = qF/2\alpha$, identical to the result of Marianer et al. [18].

The remaining issue is the determination of the effective temperature for arbitrary electric fields and ambient temperatures. There are two models as follows.

(1) *The linear model*

The gain in potential energy for any hop within the percolation cluster is partly due to thermal energy and partly due to the electric energy. The potential energy gained from thermal energy is maximized for short range hops. But the potential energy gained from the electric field is maximized for long range hops. Under the linear effective temperature model, the maximum potential energy gained from temperature-induced hops is added to the maximum potential energy gained from electric field-induced hops, i.e.,

$$T_{eff} = T_F + T. \tag{14}$$

To our knowledge, there is no rigorous justification for Eq. (14). Rather, the linear model implicitly treats the electric field in the form of T_F as a perturbation to the lattice temperature, T. The above analysis of hot carriers at $T = 0K$ is used to determine the form of the perturbation T_F. Given $T_{eff} = T_F + T$, the expression for conductivity obtained for an exponential DOS is [24]

$$\sigma = \frac{\sigma 0}{q}\left[\frac{\pi}{B_C}\frac{T0^3}{(2\alpha)^3}\frac{16T_{eff}}{(2T_{eff}-T_F)^2(2T_{eff}+T_F)^2}\right]^{T_0/T_{eff}} n^{T_0/T_{eff}}. \tag{15}$$

(2) *Non linear models*

Several authors have proposed an effective temperature of the form

$$T_{eff}^n = T^n + (\beta T_F)^n, \tag{16}$$

where $n \approx 2$ and $\beta \approx 1.4$. Marianer et al. [18] and Baranovskii et al. [15] both ran Monte Carlo simulations considering electrons hopping through an exponential DOS. The resulting electron distribution is a Fermi distribution characterized by an effective temperature given by $T_{eff}^n = T^n + (\beta T_F)^n$. Baranovskii et al. [15] found $n = 2$ and $\beta = (1.38 \pm 0.06)$ consistent with the earlier findings of Marianer et al. [18], who fit their distribution to $n = 2$ and $\beta = 1.34$.

Arkhipov et al. [19] derived the effective temperature for an algebraic DOS. Their result was obtained from the low field model of Eq. (5):

$$s_c = 2\alpha r + \frac{E - qrF - \mu}{kT}. \tag{17}$$

Similar to the percolation approach, they required that the number of sites, N_s, in Eq. (7) exceeded one (but note [8]). The DOS was taken to be

$$g(E) = g_0 \left(\frac{E-\mu}{E_0} \right)^{\gamma}, \quad E > \mu, \quad -1 < \gamma < \infty. \tag{18}$$

The effective temperature was determined to be

$$T_{\text{eff}}(T,F) = T \left[\frac{4 - (4+\gamma) f^{2+\gamma} - (5+\gamma) f^{3+\gamma} + (2+\gamma) f^{4+\gamma} + (3+\gamma) f^{5+\gamma}}{4(1-f^2)^2} \right]^{1/(1+\gamma)}, \tag{19}$$

where $f = T_F/T$. At weak fields where $f \ll 1$, and, where $\gamma > 0$, T_{eff} reduces to

$$T_{\text{eff}}(T,F) = T \left[1 + \frac{2}{1+\gamma} f^2 \right]. \tag{20}$$

At strong fields T_{eff} is simply proportional to T_F:

$$T_{\text{eff}}(T,F) = \left[\frac{3+\gamma}{4} \right]^{1/1+\gamma} T_F. \tag{21}$$

The T_{eff} derived by Arkhipov et al. [19], though different in precise form to the results of Marianer et al. [18] and Baranovskii et al. [15], is similar to Eq. (16) when $\beta = 1$ and $0 < \gamma < 1$. The various theories discussed in this section are depicted as a plot of T_F vs T at an effective temperature of 300 K in Fig. 2.

4 Comparison to Experiment

The effective temperature theories are tested against current–voltage and mobility measurements conducted by Brütting et al. and Limketkai et al. using the archetypical small molecule tris (8-hydroxyquinoline) aluminum (AlQ_3) over a wide range of electric fields and temperatures [22, 23]. The device used for the measurements is a 300 nm thick AlQ_3 film with calcium cathode and aluminum anode. AlQ_3 is an electron transporter, and electrons are injected from the calcium cathode. Calcium has a low work function and so interface effects are minimized. This is important because no injection effects are taken into account in the theory. Figure 3 shows the current–voltage data for the device. The circles represent data, and the solid lines

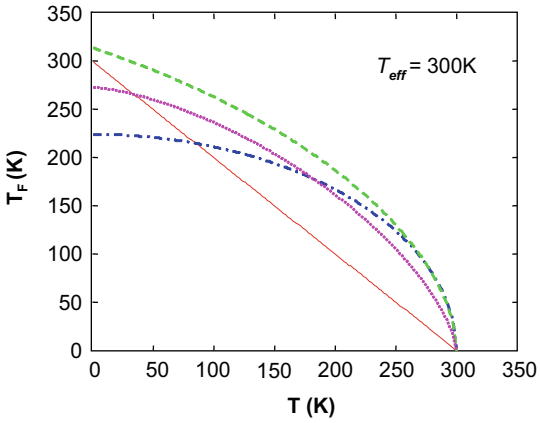

Fig. 2 T_F vs T plotted for various effective temperature theories at an effective temperature of 300 K. *Solid line:* $T_{\text{eff}} = T + T_F$; *broken line with dots:* $T_{\text{eff}}^n = T^n + (\beta T_F)^n$ where $\beta = 1.34$ and $n = 2$; *dotted line:* $\beta = 1.1$ and $n = 1.5$; *broken line:* T_{eff} transformation under the model derived by Arkhipov et al. [19]; from Eq. (19) with $\gamma = 0.7$

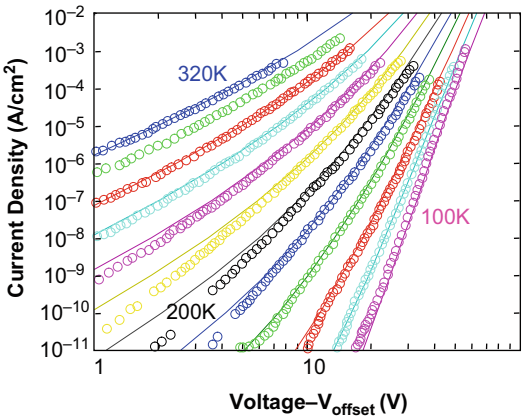

Fig. 3 Temperature dependence of *I–V* characteristics of an $Al/AlQ_3/Ca$ device, AlQ_3 thickness: 300 nm. *Symbols* are data. *Lines* are fits to theory. The offset voltage is $V_{bi} = 2$ V. As can be seen, the data fits the theory over a wide range of temperature and field. From [24]

Table 1 Fit parameters used in Fig. 3

	σ_0	α	T_0
$V_{\text{offset}} = 2$ V	2×10^3 S m^{-1}	0.575×10^{10} m^{-1}	450 K

represent the current calculated using the conductivity expression in Eq. (15) [24]. The parameters used to fit the data to theory are given in Table 1. The parameters have been calculated for an offset voltage of 2 V [24]. As can be seen from the figure, the theory accurately fits the data over a temperature range of 100–320 K.

Mobility data for AlQ_3 taken through transient electroluminescence (EL) measurements [23] has also been fitted to the theory [24]. Though the transient mobility measurement may not be exactly comparable to the predictions from the steady state theory, it is useful to compare the trends. The mobility for our theory is obtained from the conductance in Eq. (15) using $\mu = \sigma/qn$. The charge density is not experimentally defined in transient measurements, and consequently a best fit constant value of 2×10^{18} cm^{-3} is used.

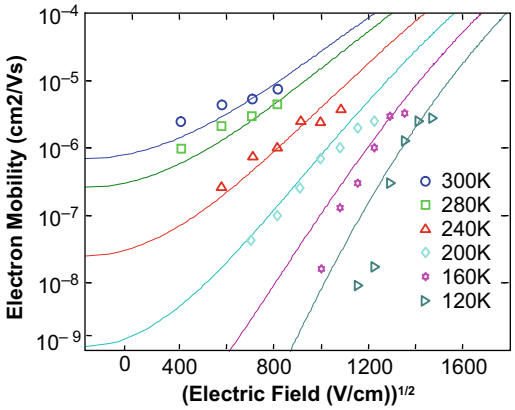

Fig. 4 Temperature and electric field dependence of charge carrier mobility obtained from transient electroluminescence measurements. Theoretical fits are shown in *solid lines*. From [24]

Figure 4 shows the fit as a log of mobility plotted against the square root of the electric field. Plotting against $\sqrt{F}$ should yield a straight line according to the Poole–Frenkel phenomenological model for mobility [9, 11]:

$$\mu = \mu_0 \exp\left[-\frac{\Theta}{kT}\right] \exp\left[B\left(\frac{1}{kT} - \frac{1}{kT_0}\right)\sqrt{F}\right], \tag{22}$$

where Θ is a temperature-independent activation barrier, and μ_0, B and T_0 are constants. It is evident that neither the data nor the theory exhibit Poole–Frenkel dependencies over a wide range of electric fields.

Next, to show the equivalence of temperature and electric field, we examine the current–voltage data as a plot of voltage vs temperature at constant conductance in Fig. 5a. The mostly straight lines are consistent with the $T_{\text{eff}} = T + T_{\text{F}}$ form of effective temperature within the temperature limits of the theory: from 100 to 300 K, and over an electric field range: of 10^5–$10^6\,\text{V}\,\text{cm}^{-1}$ over a conductivity range of seven orders of magnitude. At very low fields there is a deviation from the straight line. This is attributed to variation of the charge carrier density, n, with current. It is evident in Eq. (15) that the conductance is strongly dependent on n. The linear effective temperature theory also matches the data in this regime.

Figure 5b shows the voltage–temperature plot for AlQ_3 devices of 700 Å thickness with different cathodes at a constant conductivity of $0.1\,\text{S}\,\text{m}^{-1}$ [22, 23]. The different cathodes alter the current–voltage characteristics, either by varying the density of free charge within the AlQ_3 or by varying the injection barrier. As the work function of the cathode increases, the plots seem to show a constant voltage shift to higher voltages but again the linear form of T_{eff} is still observable.

Figure 6 shows a voltage–temperature plot for an AlQ_3 device of thickness 700 Å with a MgAg cathode [22]. The temperature range is wider for this data and a clear deviation from the linear is observed at low temperature. Some uncertainty is introduced by the possibility of an injection barrier at the MgAg/AlQ_3 interface; however, good agreement at low temperatures is evident for an effective temperature given by $T_{\text{eff}}^n = T^n + (\beta T_{\text{F}})^n$ with $n = 1.41$ and $\beta = 1.24$.

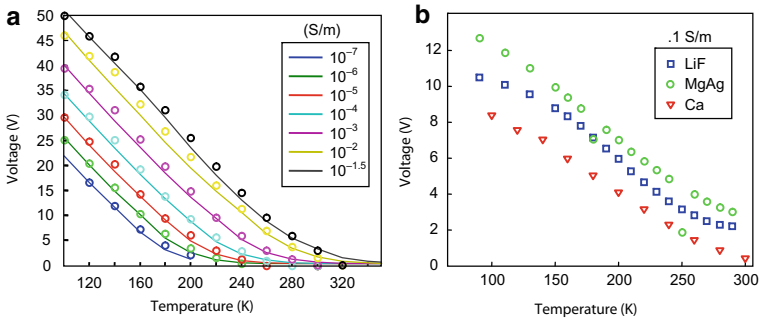

Fig. 5 **a** Voltage vs temperature as a function of conductivity for the Al/AlQ_3/Ca data (AlQ_3 thickness 300 nm) collected by Brütting et al. [23]. The *circles* are data and the *lines* are a theoretical fit. The plots are linear over a wide range of conductivity except at very low fields. This fits the linear dependence of effective temperature on field and temperature. **b** The same plot for 70 nm AlQ_3 devices with Ca, LiF and MgAg cathodes at a constant conductivity of $0.1\,\mathrm{S\,m^{-1}}$. The Ca plot is not data but a calculation for a 70 nm thick device using a linear extrapolation from thickness dependence studies for AlQ_3 in [23] and the current–voltage characteristics of the 300 nm thick AlQ_3 device in **a**. The different cathodes seem to add a constant voltage shift but the linear effective temperature dependence on field and temperature still exists. At temperatures lower than 100 K, the data veers to lower voltage values than predicted by theory

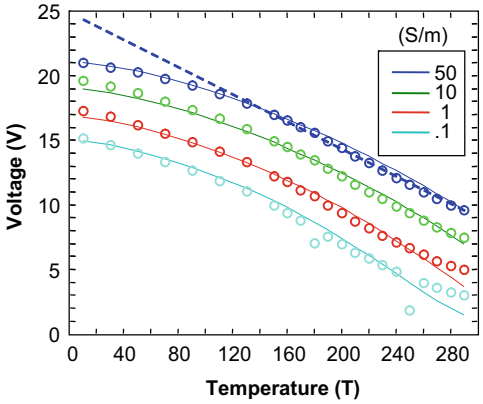

Fig. 6 Voltage vs temperature as a function of conductivity for a 700 A thick AlQ_3 device with a MgAg cathode. The *lines* are fits to theory and the *circles* are data from [19]. The fit parameters used here are ones deduced from the Brütting et al. data [23], except for $T_0 = 500\,\mathrm{K}$, and $V_{\mathrm{offset}} = 1\,\mathrm{V}$. The theoretical fit represents an effective temperature dependence given by $T_{\mathrm{eff}}^n = T^n + (\beta T_{\mathrm{F}})^n$ where $n = 1.41$ and $\beta = 1.24$. The *dashed line* shows the linear effective temperature dependence

The $T_{\mathrm{eff}}^n = T^n + (\beta T_{\mathrm{F}})^n$ form is further explored through the Brütting et al. data [23] for a 3,000 Å thick AlQ_3 device with Ca cathode. The transient mobility data (Fig. 4) are transformed under the various effective temperature models discussed in Sect. 3. Figure 7 shows a plot of the transient mobility data for various electric

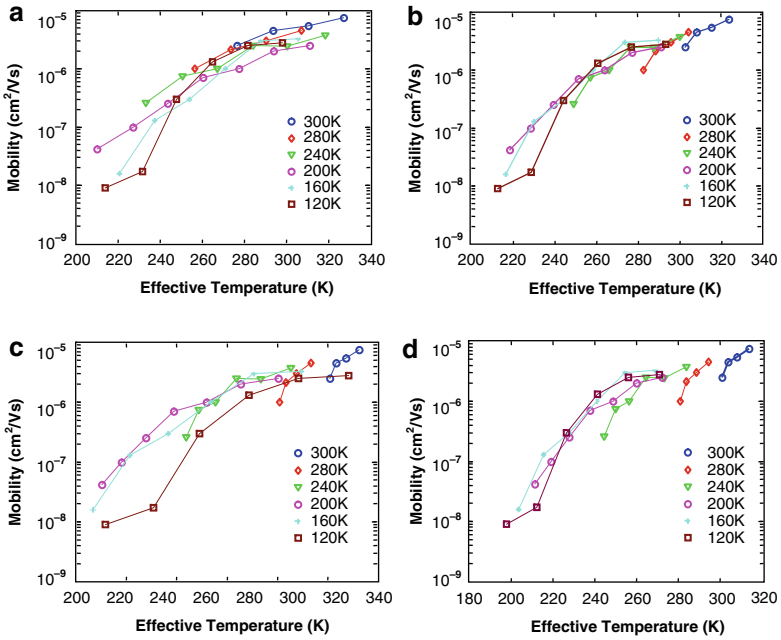

Fig. 7 The transient mobility data of Fig. 4 under various effective temperature transformations. The first four are given by $T_{\text{eff}}^{n} = T^{n} + (\beta T_{\text{F}})^{n}$ where: **a** $n = 1$, $\beta = 1$; **b** $n = 1.5$, $\beta = 1.1$; **c** $n = 2$, $\beta = 1.3$; **d** Transformation under the model derived by Arkhipov et al. [19]; from Eq. (19) with $\gamma = 0.7$

fields and temperatures vs the effective temperature. Specifically, Fig. 7a–c shows $T_{\text{eff}}^{n} = T^{n} + (\beta T_{\text{F}})^{n}$ with $n = 1$, 1.5 and 2 and optimal β values [32]. The β has been optimized to fit each transformation, except for $n = 1$, where it is taken as $\beta = 1$. If the mobility is a function of the effective temperature, then all the data (for all temperatures and fields) should collapse onto a single function. Figure 7d shows the transformation under the expression in Eq. (19) derived by Arkhipov et al. [19] with an optimized value of $\gamma = 0.7$.

5 Discussion

Comparisons with data demonstrate that the effective temperature model shows promise: both the steady state current–voltage data and the mobility data exhibit universal behavior parameterized by an effective temperature. Data are observed to fit the effective temperature model over a wide range of temperatures, carrier densities, and electric fields. Figure 6 confirms that the $T_{\text{eff}}^{n} = T^{n} + (\beta T_{\text{F}})^{n}$ model with $n \approx 1.5$ provides the best fit over the widest range of temperatures, albeit with the addition of the empirical parameter n [32]. But for engineering purposes, where performance near room temperature is most important, the linear model provides the best fit;

compare Fig. 7a, b. It is observed to work well when T_F is a small perturbation ($T_F \ll T$). The linear effective temperature model fails at lower temperatures when the electric field temperature, T_F, approaches the lattice temperature, T.

Despite the success of the effective temperature models in describing charge transport in AlQ_3, each model possesses an uncertain physical foundation. The linear theory essentially treats the electric field as a perturbation and is experimentally observed to be valid only above $T \approx 100\,K$. Despite the apparent failure of the model at low temperatures, the form of T_F is determined using arguments at $T = 0\,K$. Its success at room temperature may then be due to the implicit combination of a fit parameter and α, the orbital decay constant. Since quantum chemical calculations can be used to determine α, further studies should be able to resolve this. The $T_{eff}^n = T^n + (\beta T_F)^n$ models are closest to universal but they are fundamentally empirical. Numerical studies have also suggested that even $T_{eff}^n = T^n + (\beta T_F)^n$ models cannot be truly universal because β apparently varies when the effective temperature is used to simulate transient or steady state currents [33]. Lastly, the theory of Arkhipov et al. [19] applies only to algebraic densities of states, and provides a relatively poor fit to the data. The later theory is notable, however, for suggesting that the form of the effective temperature may depend on the DOS.

The linear model has also been criticized by Cleve et al. [33] as possessing incorrect asymptotic behavior at low electric fields. They require that

$$\left.\frac{d\sigma}{dF}\right|_{F\to 0} = \left.\frac{d\sigma}{dT_{eff}}\frac{dT_{eff}}{dF}\right|_{F\to 0} = 0. \tag{23}$$

Their concern was $dT_{eff}/dF \neq 0$ in the linear effective temperature model. Physically, we expect that a successful model of conductance should smoothly evolve from electric field-independence at $F = 0$ to increasing electric field-dependent nonlinearity at $F > 0$. Plots of the charge carrier mobility using the linear effective temperature model in Fig. 4 are consistent with the expected behavior. Moreover, we note that the effective temperature depends on the *magnitude* of the electric field. Hence, as required by symmetry arguments,

$$\frac{T_{eff}(\delta/2) - T_{eff}(-\delta F/2)}{\delta F} = 0, \quad \delta F > 0. \tag{24}$$

In any case, comparisons with data show no evidence of failure of the linear model at low electric fields. In fact, the linear model arguably fits the low electric field data better than the $T_{eff}^n = T^n + (\beta T_F)^n$ models.

6 Conclusion

It has been established that percolation theory can successfully explain the mobility in organic semiconductors at low electric fields. Organic semiconductor devices, however, often operate at larger electric fields. The electric field distorts the

distribution of carriers within the organic semiconductor, leading to a substantial change in the charge carrier mobility. Effective temperature models seek to describe such complex hot carrier phenomena with a single effective temperature dependent on the electric field and the lattice temperature. It remains unclear whether a truly universal effective temperature theory is possible [33]. Nevertheless, comparisons to data from the archetype small molecular weight electron transport material AlQ_3 yield three important conclusions. First, the most accurate effective temperature model over a wide range of temperatures is the empirical relation $T_{\text{eff}}^n = T^n + (\beta T_{\text{F}})^n$ with $n \approx 1.5$ [32]. Second, the simple linear model is arguably superior to the empirical models near room temperature. It also replaces constants of unclear physical origin with parameters that may potentially be obtained using quantum chemical simulations. Third the linear effective temperature model is simply understood as a first order perturbation in the carrier distribution, i.e., it is expected to be valid for $T_{\text{F}} \ll T$, which typically corresponds to the operating conditions of most organic devices. Thus, for organic semiconductor engineers concerned with the rational design of OLEDs and OPVs, the linear model of effective temperature may provide the most practical description of the electric field dependence of charge carrier mobility.

References

1. Anderson PW (1958) Absence of diffusion in certain random lattices. Phys Rev 109:1492
2. Miller A, Abrahams E (1960) Impurity conduction at low concentrations. Phys Rev 120:745
3. Holstein T (1959) Studies of polaron motion. Part 1. The molecular-crystal model. Ann Phys 8:325
4. Holstein T (1959) Studies of polaron motion. Part II. The 'small' polaron. Ann Phys 8:343
5. Burrows PE, Shen Z, Bulovic V, McCarty DM, Forrest SR, Cronin JA, Thompson ME (1996) Relationship between electroluminescence and current transport in organic heterojunction light-emitting devices. J Appl Phys 79:7991
6. Tanase C, Blom PWM, de Leeuw DM (2004) Origin of the enhanced space-charge-limited current in poly(*p*-phenylene vinylene). Phys Rev B 70:193202
7. Tanase C, Meijer EJ, Blom PWM, de Leeuw DM (2003) Unification of the hole transport in polymeric field-effect transistors and light-emitting diodes. Phys Rev Lett 91:216601
8. Coehoorn R, Pasveer WF, Bobbert PA, Michels MAJ (2005) Charge-carrier concentration dependence of the hopping mobility in organic materials with Gaussian disorder. Phys Rev B 72:155206
9. Pasveer WF, Cottaar J, Tanase C, Coehoorn R, Bobbert PA, Blom PWM, de Leeuw DM, Michels MAJ (2005) Unified description of charge-carrier mobilities in disordered semiconducting polymers. Phys Rev Lett 94:206601
10. Vissenberg MCJM, Matters M (1998) Theory of the field-effect mobility in amorphous organic transistors. Phys Rev B 57:12964
11. Bässler H (1993) Charge transport in disordered organic photoconductors. Phys Status Solidi B 175:15
12. Ambegaokar V, Halperin BI, Langer JS (1971) Hopping conductivity in disordered systems. Phys Rev B 4:2612
13. Shklovskii BI (1973) Hopping conduction in semiconductors subjected to a strong electric-field. Sov Phys Semiconductors USSR 6:1964
14. Shklovskii BI, Levin EI, Fritzsche H, Baranovskii SD (1990) In: Fritzsche H (ed) Advances in disordered semiconductors, vol. 3, Transport, correlation and structural defects. World Scientific, Singapore, pp 161–191

15. Baranovskii SD, Cleve B, Hess R, Thomas P (1993) Effective temperature for electrons in band tails. J Non Cryst Sol 166:437
16. Lampert MA, Mark P (1970) Current injection in solids. Academic, New York
17. Ioannidis A, Forsythe E, Gao Y, Wu MW, Conwell EM (1998) Current-voltage characteristics of organic light emitting diodes. Appl Phys Lett 72:3038
18. Marianer S, Shklovskii BI (1992) Effective temperature of hopping electrons in a strong electric-field. Phys Rev B 46:13100
19. Arkhipov VI, Emelianova EV, Adriaenssens GJ (2003) Field-dependent effective temperature and variable range hopping: application to dark dc conductivity in doped a-Si: H. J Appl Phys 93:6150
20. Tang CW, VanSlyke SA (1987) Organic electroluminescent diodes. Appl Phys Lett 51:913
21. Baldo MA, Forrest SR (2001) Interface limited injection in amorphous organic semiconductors. Phys Rev B 64:085201
22. Limketkai BN, Baldo MA (2005) Charge injection into cathode-doped amorphous organic semiconductors. Phys Rev B 71:085207
23. Brütting W, Berleb S, Mückl AG (2001) Device physics of organic light-emitting diodes based on molecular materials. Org Electron 2:1
24. Limketkai BN, Jadhav P, Baldo MA (2007) Electric field dependent percolation model of charge carrier mobility in amorphous organic semiconductors. Phys Rev B 75:113203
25. Movaghar B, Grunewald M, Ries B, Bassler H, Wurtz D (1986) Diffusion and relaxation of energy in disordered organic and inorganic materials. Phys Rev B 33:5545
26. Vissenberg MCJM (1999) Opto-electronic properties of disordered organic semiconductors. University of Leiden, The Netherlands
27. Tal O, Rosenwaks Y, Preezant Y, Tessler N, Chan CK, Kahn A (2005) Direct determination of the hole density of states in undoped and doped amorphous organic films with high lateral resolution. Phys Rev Lett 95:256405
28. Celebi K, Jadhav PJ, Milaninia KM, Bora M, Baldo MA (2008) The density of states in thin film copper phthalocyanine measured by Kelvin probe force microscopy. Appl Phys Lett 93:083308
29. Hirao A, Nishizawa H, Sugiuchi M (1995) Diffusion and drift of charge carriers in molecularly doped polymers. Phys Rev Lett 75:1787
30. Sahimi M (1994) Applications of percolation theory. Taylor and Francis, London
31. Pike GE, Seager CH (1974) Percolation and conductivity – Computer study 1. Phys Rev B 10:1421
32. Jansson F, Baranovskii SD, Gebhard F, Osterbacka R (2008) Effective temperature for hopping transport in a Gaussian density of states. Phys Rev B 77:195211
33. Cleve B, Hartenstein B, Baranovskii SD, Scheidler M, Thomas P, Baessler H (1995) High-field hopping transport in band tails of disordered semiconductors. Phys Rev B 51:16705

http://www.springer.com/978-3-642-04537-0

Organic Electronics
Meller, G.; Grasser, T. (Eds.)
2010, XIV, 330 p. 178 illus., 50 illus. in color., Hardcover
ISBN: 978-3-642-04537-0